Polarization Rotation and the Third Stokes Parameter: The Effects of Spacecraft Attitude and Faraday Rotation

Thomas Meissner and Frank J. Wentz

***Abstract*—The third Stokes parameter of ocean surface brightness temperatures measured by the WindSat instrument is sensitive to the rotation angle between the polarization vectors at the ocean surface and the instrument. This rotation angle depends on the spacecraft attitude (roll, pitch, yaw) as well as the Faraday rotation of the electromagnetic radiation passing through the Earth's ionosphere. Analyzing the WindSat antenna temperatures, we find biases in the third Stokes parameter as function of the along-scan position of up to 1.5 K in all feedhorns. This points to a misspecification of the reported spacecraft attitude. A single attitude correction of $-0.16°$ roll and 0.18° pitch for the whole instrument eliminates all the biases. We also study the effect of Faraday rotation at 10.7 GHz on the accuracy of the third Stokes parameter and the sea surface wind direction retrieval and demonstrate how this error can be corrected using values from the International Reference Ionosphere for the total electron content when computing Faraday rotation.**

***Index Terms*—Faraday rotation, spacecraft attitude, Stokes vector, WindSat.**

I. Introduction

THE retrieval of sea surface wind direction from WindSat measured brightness temperatures requires a very accurate knowledge of the third Stokes parameter, which is one of the basic inputs for any wind vector retrieval algorithm.

The four-component brightness temperature Stokes vector is defined as

$$\begin{pmatrix} I \\ Q \\ U \\ S_4 \end{pmatrix} = \begin{pmatrix} \langle E_V \cdot E_V^* + E_H \cdot E_H^* \rangle \\ \langle E_V \cdot E_V^* - E_H \cdot E_H^* \rangle \\ 2\mathrm{Re}\langle E_V \cdot E_H^* \rangle \\ 2\mathrm{Im}\langle E_V \cdot E_H^* \rangle \end{pmatrix} = \begin{pmatrix} T_V + T_H \\ T_V - T_H \\ T_P - T_M \\ T_L - T_R \end{pmatrix}. \quad (1)$$

Here $E_p = \vec{E} \cdot \hat{p}$ is the component of the electric field in polarization direction $\hat{p}$ and T_p is the brightness temperature in polarization direction $\hat{p}$, which stands for V (vertical), H (horizontal), $\mathrm{P} = 1/\sqrt{2}(\mathrm{V} + \mathrm{H})$ (+45 linear), $\mathrm{M} = 1/\sqrt{2}(\mathrm{V} - \mathrm{H})$ (−45 linear), $\mathrm{L} = 1/\sqrt{2}(\mathrm{V}+\mathrm{iH})$ (left circular) or $\mathrm{R} = 1/\sqrt{2}(\mathrm{V}-\mathrm{iH})$ (right circular) (see Fig. 1). The $\langle \ldots \rangle$ denotes the time average.

The Stokes vector that is measured by the instrument differs from the Stokes vector at the sea surface, because the polarization vectors for the electric fields in the Earth and spacecraft (S/C) coordinate systems are rotated by a polarization rotation angle φ. If $\hat{k}$ denotes the propagation unit vector of the electromagnetic radiation pointing from Earth to S/C and $\{\hat{V}, \hat{H}, \hat{k}\}$ is the Earth polarization system and $\{\hat{V}', \hat{H}', \hat{k}\}$ the S/C polarization basis [see Fig. 1 and (30) and (31)], then the electric field components in the Earth and S/C system are related by

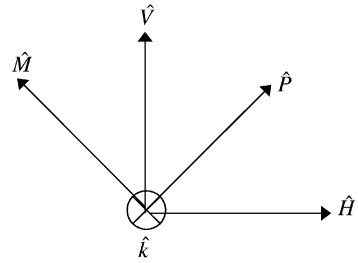

Fig. 1. Polarization unit vectors. The propagation vector $\hat{k}$ points into the plane.

$$\begin{pmatrix} (\vec{E} \cdot \hat{V}') \\ (\vec{E} \cdot \hat{H}') \end{pmatrix} = \begin{pmatrix} \cos(\varphi) & -\sin(\varphi) \\ \sin(\varphi) & \cos(\varphi) \end{pmatrix} \begin{pmatrix} (\vec{E} \cdot \hat{V}) \\ (\vec{E} \cdot \hat{H}) \end{pmatrix}. \quad (2)$$

The rotation (2) results in a rotation of the Stokes parameters and that have been defined in (1)

$$\begin{pmatrix} Q' \\ U' \end{pmatrix} = \begin{pmatrix} \cos(2\varphi) & -\sin(2\varphi) \\ +\sin(2\varphi) & \cos(2\varphi) \end{pmatrix} \begin{pmatrix} Q \\ U \end{pmatrix}. \quad (3)$$

The first Stokes parameter I and the fourth Stokes parameter S_4 remain unchanged.

The third Stokes parameter U has a peak-to-peak amplitude of about 3 K at intermediate and high wind speeds over the whole range of wind directions relative to the azimuthal look. As a typical value for the error in U, we can take the root mean square (RMS) of the difference between the measured value of U and its theoretical prediction from the radiative transfer model (RTM). For the relevant WindSat channels, this difference is on the order of 0.25 K. This value accounts for sensor errors (e.g., radiometer noise) and errors in the RTM function but assumes otherwise perfect alignment of the polarization vectors. On the other hand, the value for the second Stokes parameter Q is on the order of 75 K for typical ocean scenes. From this it follows, that even small errors in the polarization rotation angle φ introduce a significant error into the third Stokes parameter by means of (3): with $Q = 75$ K, an inaccuracy in of 0.1° leads to an error in of about 0.26 K, which is the same size as the errors due to radiometer noise and RTM inaccuracies. Moreover, the retrieval of sea surface temperature (SST) requires a very high accuracy for the V-pol and H-pol brightness temperatures

Manuscript received January 31, 2005; revised August 2, 2005.

The authors are with Remote Sensing Systems, Santa Rosa, CA 95401 USA (e-mail: meissner@remss.com; frank.wentz@remss.com).

Digital Object Identifier 10.1109/TGRS.2005.858413

in the two lowest bands. An error of 0.1 K in the 6.8-GHz V-pol brightness temperature translates typically into an error of 0.2 K in the retrieved SST.

It is the aim of this investigation to study errors in the polarization rotation angle that occur due to the following.

1) *Misspecifications in the S/C attitude (roll, pitch, and yaw):* These three parameters determine the orientation of the internal S/C coordinate system with respect to the coordinate system defined by the orbital plane (radial vector, velocity, angular momentum).
2) *Faraday Rotation:* Rotation of the polarization vector of electromagnetic radiation traveling through the Earth's ionosphere in the geomagnetic field. This effect increases with the inverse square of the radiation frequency and is therefore most important for the lowest frequency at which WindSat measures the third Stokes parameter, which is 10.7 GHz.

We will also show how to correct for both of these errors and thus improve the accuracy for the third Stokes parameter, which is necessary to obtain accurate wind vector retrievals.

Our paper is organized as follows. In Section II, we describe the essential characteristics of the dataset of WindSat antenna temperatures that we have used for this study and its conversion into brightness temperature Stokes vector components. We briefly summarize the main features of the radiative transfer model (RTM) function and how to obtain the geophysical input parameters for computing it. The RTM function is used for eliminating geophysical variability in the measured brightness temperatures. In Section III, we analyze biases in the third Stokes parameters as a function of along-scan position. We show that these biases arise as result of a misspecification in the S/C attitude. They can be eliminated by introducing a correction to the S/C attitude parameters. Section IV discusses the Faraday rotation at 10.7 GHz and its effect on the third Stokes parameter and the WindSat wind vector retrievals. We compute Faraday rotation using the International Geomagnetic Reference Field (IGRF 9) and values for the total electron content from the International Reference Ionosphere (IRI 2001). We also show how to include Faraday rotation in the computation of the third Stokes parameter. A short summary is given in Section V.

II. Study Dataset

A. WindSat Antenna Temperatures and Geolocation

The WindSat antenna temperature data records (TDR version 146AFBBDA [1], [2]) contain measured antenna temperatures for the 22 channels (6.8 VH, 10.7 VH PM LR, 18.7 VH PM LR, 23.8 VH, 37.0 VH PM LR), together with observation time and the geolocation parameter, which are as follows:

1) geodetic latitude (LAT) of the observed Earth cell;
2) longitude (LON) of the observed Earth cell;
3) Earth incidence angle (EIA) θ;
4) azimuth angle α of the looking direction relative to geographic north;
5) rotation angle φ_P between the Earth and S/C polarization basis vectors.

These basic five geolocation parameters are uniquely determined by the following.

TABLE I
Number of Sample Lags, for Which the Feedhorns in Polarimetric Bands Observe the Same Earth Cell

Band	VH/LR	VH/PM	LR/PM
10.7	7	14	7
18.7	7	14	7
37.0	12	24	12

A) The S/C location, which is given by the location vector $\vec{R}_{\mathrm{S/C}}$ pointing from the Earth's center to the S/C (in either an inertial or Earth fixed Cartesian coordinate system), or, equivalently, S/C latitude, longitude and altitude.
B) The orientation of the coordinate axes $\{\hat{X}, \hat{Y}, \hat{Z}\}$ that are fixed to the S/C relative to the inertial or Earth fixed axes. This is commonly described by the three Euler angles roll r, pitch p, and yaw y.
C) The boresight nadir angle θ_n, which is a constant for each of the 11 feedhorns.
D) The antenna boresight looking azimuth ω (also called scan angle). In our convention, it is defined as zero when the radiometer is looking forward, positive when looking left of forward, and negative when looking right of forward. In each scan, ω varies synchronously with the scan position.

The basic relations and our conventions for these parameters and the steps that are involved to determine 1–5 from A–D are summarized in the Appendix.

The TDR dataset itself does not contain values for the nadir looking angles, nor does it give values for roll, pitch, or yaw. A fit value for θ_n for each feedhorn can be easily obtained from the observed geolocation parameters 1–5. Furthermore, assuming that they do not change during a scan, the attitude parameters r, p and can y be fitted for each scan from the observed values for the basic geolocation parameters 1–5.

We also compute the sun glint angle, which is the difference between the vector of the incident sun radiation onto the observation cell and the direction of specular reflection. To avoid sun glitter, we discard any observation for which the sun glint angle is less than 25°. Similarly, we can eliminate 10.7-GHz radio-frequency interference (RFI) from the two known geostationary television satellites ASTRA and HOTBIRD that are orbiting at 13°E and 19°E, respectively. Observations are discarded for which the RFI glare angle, which is defined as the difference between the vector of the incident radio frequency radiation onto the observation cell and the direction of specular reflection, is smaller than 25°.

B. Cross Polarization Correction

In order to obtain the Stokes Vectors for the 10.7-, 18.7-, and 37.0-GHz polarimetric bands, the Stokes parameters within each of the polarimetric bands must be spatially collocated to the same Earth cell. To a very good approximation, the three horns in a polarimetric frequency band observe the same Earth cell at three different times that are separated by a constant lag. The desired spatial collocation can thus be obtained by an appropriate time shift of each observation. The WindSat instrument design is such that, to a very good approximation, the time delay is an integer multiple of the sampling rate (Table I).

The calculation of the brightness temperatures T_B at the ocean surface from the antenna temperatures T_A that are measured by WindSat involves three basic corrections.

1) Antenna Spillover Correction: The feedhorn spillover accounts for power losses between the reflector and the feedhorns as well as power entering the feedhorn from cold space rather than from the feedhorn

$$T_A = \eta T'_A + (1-\eta)T_C \tag{4}$$

and therefore

$$T'_A = \frac{T_A - (1-\eta)T_C}{\eta}. \tag{5}$$

Here, T'_A corresponds to the radiation at the reflector, T_A corresponds to the radiation entering the feedhorns and $T_C = 2.7K$ is the cold space temperature. We are using the values for the spillover factor η for each of the 22 channels given by [3].

2) Polarization Leakage Correction: The antenna temperature T'_A in polarization direction q is not identical to the brightness temperature T'_B in polarization direction q arriving at the antenna but has also small components from other polarization directions. The cross-pol matrix M_{pq} describes the coupling from Stokes component q into Stokes component p

$$(T'_A)_p = M_{pq} \cdot (T'_B)_q. \tag{6}$$

For the three polarimetric bands, the polarization direction indexes p and q run over all four Stokes components, whereas for the two nonpolarimetric bands (6.8 and 23.8 GHz) they include only V-pol and H-pol. The cross-pol correction matrix M_{pq}^{-1}, which is the inverse of M_{pq}, has been determined in [1], [3].

3) Polarization Rotation Correction: This corrects the rotation between the Earth and S/C polarization bases by the polarization rotation angle φ_P as mentioned in Section I. Applying (3) gives the relation between the Stokes components (1) of T'_B (S/C) and T_B (Earth)

$$\begin{aligned} I' &= I \\ \begin{pmatrix} Q' \\ U' \end{pmatrix} &= \begin{pmatrix} \cos(2\varphi_P) & -\sin(2\varphi_P) \\ +\sin(2\varphi_P) & \cos(2\varphi_P) \end{pmatrix} \begin{pmatrix} Q \\ U \end{pmatrix} \\ S'_4 &= S_4 \end{aligned} \tag{7}$$

which can be easily inverted. For the nonpolarimetric bands the third Stokes vector is not measured and we assume $U' = 0$ when applying the inverse transformation of (7). For the moment, we have not yet applied a correction for Faraday rotation. Faraday rotation has the same form as (7) and we will come back to it in detail in Section IV.

C. Radiative Transfer Model Function

When analyzing the WindSat brightness temperatures T_B it is necessary to remove any geophysical variability that arises due to changes in the following:

a) atmospheric profiles for temperature, water vapor, and liquid cloud water, which determine the attenuation of the electromagnetic radiation through the atmosphere;

b) ocean surface parameters that determine the emissivity of the observed Earth cell: sea surface temperature (SST), sea surface salinity (SSS), sea surface wind speed (SSWS), and direction (SSWD) (relative to look direction).

The best way to achieve this is to consider the difference between T_B and the value calculated by the RTM function F. For our purpose, it is sufficient to consider a simplified RTM that does not depend on the full atmospheric profiles, but only on the columnar values for water vapor and liquid cloud water. For the along-scan bias analysis in Section III we will consider averages over a large numbers of samples, so that possible small inaccuracies in the RTM tend to cancel out. Therefore, our analysis does not require a very highly accurate RTM. The isotropic (wind direction independent) part of our RTM is described in [4]. For the wind direction signal, we have used [5] for V- and H-pol in all three polarimetric bands and [6] for the third Stokes parameters at 18.7 and 37.0 GHz. As a first guess for the third Stokes parameter at 10.7 GHz, we have taken the value at 18.7 GHz and multiplied it by a factor of 0.6, which follows the frequency behavior of the V- and H-pol wind direction signal [5]. Our results of a consistent analysis of the wind direction signal for all four Stokes parameters using WindSat brightness temperatures will be reported elsewhere.

D. Geophysical Parameters

The computation of the RTM function F requires the knowledge of the geophysical surface and atmospheric parameters mentioned above at the location and time of the WindSat observation. For this purpose, we collocate the WindSat dataset with Earth observations from numerical weather prediction models, climatologies, and measurements from other satellites as follows.

1) SST is obtained from the Reynolds optimum interpolated (OI) product [7], a weekly 1° field derived from *in situ* and infrared satellite SST observations.
2) SSS is obtained from the World Ocean Atlas WOA98 [8].
3) SSWS and SSWD are obtained from the National Centers for Environmental Prediction (NCEP) General Data Assimilation system (GDAS) 6-h 1° analysis.[1]

   The products 1–3 are trilinearly (latitude, longitude, and time) interpolated to the location and time of the WindSat observation.
4) In order to obtain values for columnar water vapor and liquid cloud water we require that the WindSat observation lies within 90 min of one of the $1/4^\circ$ cells containing a rain-free observation from one of the microwave imager satellites that are processed by Remote Sensing Systems (http://www.remss.com): the Special Sensor Microwave Imager (SSM/I), the Tropical Rainfall Mission Microwave Imager (TMI), and the Advanced Microwave Scanning Radiometer (AMSR-E). We use the satellite observation that is closest in time to the WindSat observation. The requirement for a rain-free observation is that the columnar cloud liquid water from one of the microwave imager is less than 0.18 mm [4], [9].

[1]Available at ftp://ftpprd.ncep.noaa.gov/pub/data/nccf/com/gfs/prod/gdas.

III. Along-Scan Scan Biases and Attitude Correction

A. Along-Scan Biases

The impact of sensor attitude on the polarization rotation angle and polarimetric brightness temperature has been demonstrated and studied for airborne microwave radiometers [10]. Aside from sign conventions, we are using the same mathematical relations between sensor attitude and polarization rotation angle as [10]. It is the aim of our study to trace and correct an actual error in the attitude of the WindSat instrument by analyzing along-scan biases in the brightness temperature measurements. We show how this can be achieved by comparing brightness temperatures that were measured by WindSat with those that were computed from our highly accurate radiative transfer model.

The left panels of Fig. 2 show the difference between the WindSat brightness temperature T_B and our RTM function F for ocean observations [4]. The results shown are averages over WindSat orbits rev # 3600 through rev # 4600 for the three fully polarimetric bands (10.7, 18.7, and 37.0 GHz) and are plotted as a function of the antenna boresight azimuth (scan angle) ω. For each band, we show the polarization combination $V - H/2$ and the third Stokes parameter U. Because small errors in the atmospheric parameters (columnar water vapor and columnar liquid cloud water) or the atmospheric part of the RTM can introduce a large error in F, we are using the difference $V - H/2$ rather than V-pol and H-pol themselves, as this combination is much less sensitive to atmospheric uncertainties. The reason for this is that at the incidence angles and frequencies under consideration the reflectivity of the ocean surface is about twice as large for H-pol than for V-pol and therefore atmospheric fluctuations in the brightness temperatures tend to cancel out when taking $V - H/2$.

Large parts of the scan are reserved for calibration and hence do not contain Earth observations but rather hot and cold calibration counts. In order to avoid any roll off in the brightness temperatures that occurs in the vicinity of the calibration targets, we only use observations well away from the calibration zones. The two segments in Fig. 2 indicate the scan positions where Earth measurements were taken during both the forward look and the aft looks. The larger segment corresponds to the forward look and the smaller segment to the aft look. We have fitted sinusoidal functions (dotted for $V - H/2$ and dashed for U) of the form $A_0 + A_1 \sin(\omega - \omega_0)$ to each curve. The overall shifts A_0 are of no importance for the present analysis. They result from calibration errors that are independent of the along-scan position such as for example errors in the reported spillover η or errors in the RTM. These absolute offsets will be handled at a later point when performing a full calibration of the WindSat brightness temperatures.

Our findings can be summarized as follows.

1) For all three polarimetric bands we find biases for $V - H/2$ and U. The size of the biases is between 0.5–1.0 K. The biases are present within both the forward and aft looks.
2) For all three polarimetric bands the forward and aft look differ by 1.0–1.5 K. This applies to both $V - H/2$ and U.
3) The standard deviations of $V - H/2$ and U are about 0.5 K each, and the values do not change over the scan. However, the accuracy of the fit for the amplitudes in Fig. 2 is much better. The reason for this is that a large number of events (more than 900 000) enters for each scan position in Fig. 2, which leads to an estimated error of less than 0.1 K in the fitted amplitudes.
4) In each band, the oscillations of $V - H/2$ and U have a relative phase of 90° as function of ω.
5) The sign and the phase angle of the oscillation are approximately the same for all three bands. The amplitude A_1 of the sinusoidal form differs among the three bands.
6) Although not shown here, the two nonpolarimetric bands (6.8 and 23.8 GHz) display the same oscillation of $V - H/2$ as shown in Fig. 2.
7) We have obtained essentially the same results when performing the analysis for different sets containing on the order of 1000 orbits during the time period between July 2003 and April 2004 than the ones used in Fig. 2.

As stated in Section I, an error in V-pol and H-pol and the third Stokes parameter of this size would pose a very serious problem for any algorithm that tries to retrieve sea surface temperature or the sea surface wind vector. It is therefore necessary to find a reliable way to correct these biases.

B. Earth Incidence Angle and Polarization Rotation Angle Errors

The observed along-scan biases in $V - H/2$ and U can be explained by misspecifications of the Earth incidence angle (EIA) θ and polarization rotation angle φ_P that were reported in the WindSat TDR set [1], [2]. A difference $\Delta\theta = \theta_{\rm true} - \theta_{\rm rep}$ leads to an along-scan bias

$$\Delta\left(T_{\rm BV} - \frac{1}{2}T_{\rm BH}\right) = \frac{\partial\left(F_V - \frac{1}{2}F_H\right)}{\partial\theta}\Delta\theta. \tag{8}$$

In accordance with (2), a difference $\Delta\varphi = \varphi_{P\rm true} - \varphi_{P\rm rep}$ translates into an along-scan bias in the third Stokes parameter

$$\Delta U \approx Q\sin(2\Delta\varphi) \approx 2Q\Delta\varphi \tag{9}$$

assuming that $\Delta\varphi$ is small and measured in radians. Using (8) and (9) we can easily calculate $\Delta\theta$ and $\Delta\varphi$ from the corresponding values for $\Delta(T_{\rm BV} - T_{\rm BH}/2)$ and ΔU from Fig. 2. In doing so we have subtracted the overall biases A_0 and inserted values for $^{\partial F}/_{\partial\theta}$ and Q that were computed from the RTM for typical ocean–atmosphere scenes (Table II). The result is shown in Fig. 3. The most important feature is the fact that the curves are almost identical for all three polarimetric bands. That means that the along-scan biases can be explained by a difference $\Delta\theta$ in the EIA and a difference $\Delta\varphi$ in the polarization rotation angle that is phase shifted by 90° in ω relative to the $\Delta\theta$. $\Delta\theta$ and $\Delta\varphi$ are the same for all three polarimetric bands. Though not shown, this is also true for the two nonpolarimetric bands as far as $\Delta\theta$ is concerned. The results for $\Delta\theta$ and $\Delta\varphi$ in Fig. 3 can be fitted by

$$\begin{aligned}\Delta\theta(\omega) &= \Delta\theta_0\sin(\omega - \omega_0)\\ \Delta\varphi(\omega) &= \Delta\varphi_0\sin(\omega - \omega_0 + 90^\circ)\end{aligned} \tag{10}$$

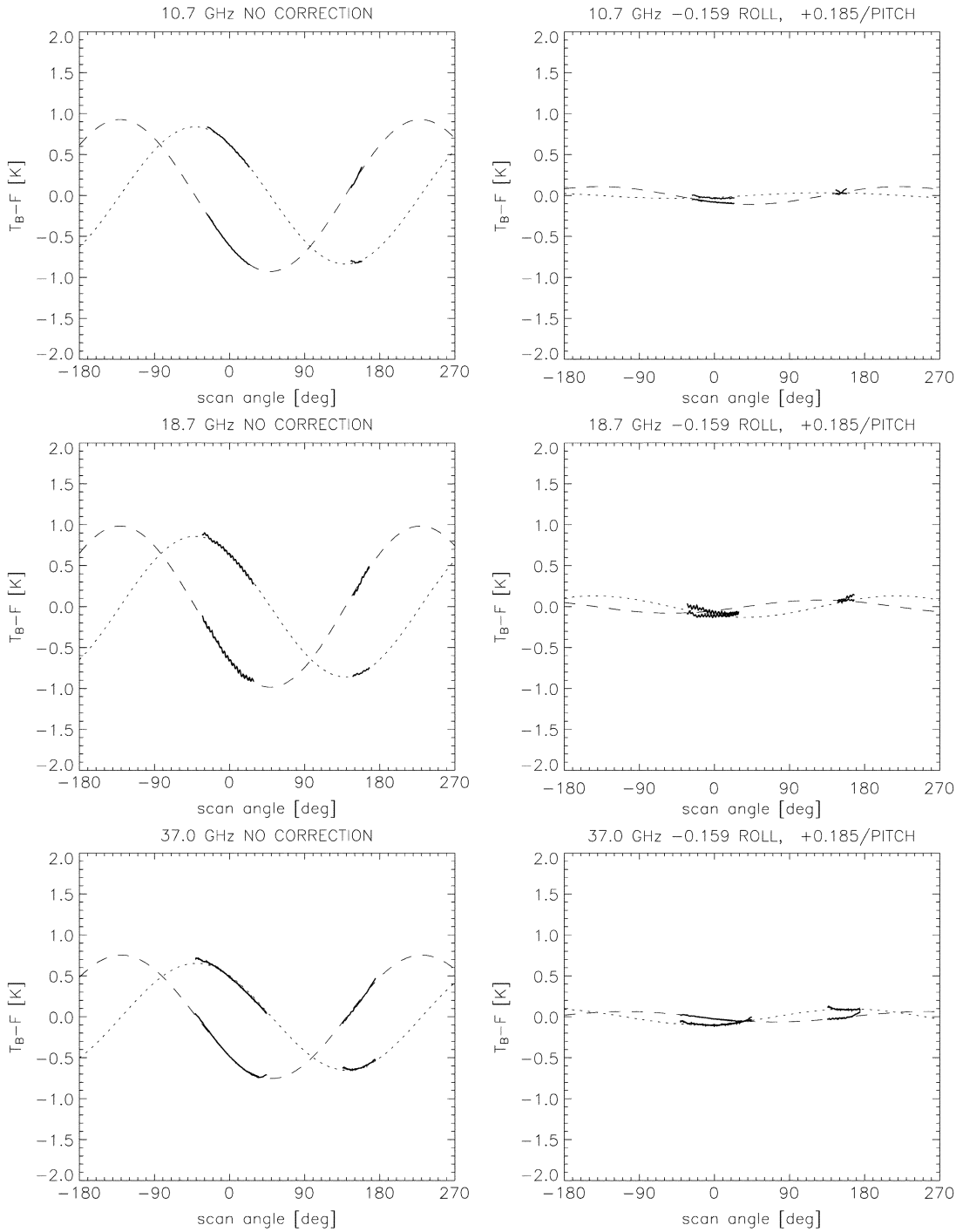

Fig. 2. Difference between measured and computed ocean brightness temperatures (along-scan biases) for (dotted line) the combination $V - H/2$ and (dashed line) the third Stokes parameter as function of the antenna boresight looking azimuth (scan angle) at 10.7, 18.7, and 37.0 GHz after removing and overall shift. The full segments indicate the scan positions with actual measurements. The dotted and dashed curves are fits to a sinusoidal function. The plot averages orbits rev # 3600–rev # 4600. The left panel shows the results from the WindSat TDR set [1], [2], the right panel after the roll/pitch error has been corrected.

with $\Delta\theta_0 = 0.33°, \Delta\varphi_0 = 0.34°$, and $\omega_0 = -130.5°$. The error for the amplitudes for $V - H/2$ and U of less than 0.1 K translates into an error of about 0.04° for $\Delta\theta_0$ and 0.04° for $\Delta\varphi_0$.

C. Roll and Pitch Correction

The most likely explanation for the errors $\Delta\theta$ and $\Delta\varphi$ is a misspecification of the S/C roll and pitch that were used for calculating the viewing geometry. It is not difficult to show that a S/C roll of $-0.16°$ and a S/C pitch of $+0.18°$ (for definitions and convention see the Appendix) would produce an oscillation in θ and φ_P very similar to that shown in Fig. 3. The error in the determination of these values is less than 0.02°. As a final check, we subtracted 0.16° from the reported S/C roll angle and added 0.18° to the S/C pitch angle. Based on 7) in Section III, we assume these offsets were constant over the entire time period considered herein. The above along-scan bias analysis was then repeated. The results are shown in the right panel of Fig. 2.

TABLE II
VALUES FOR $(\partial(F_v - F_H/2))/(\partial\theta)$ AND Q FOR TYPICAL OCEAN–ATMOSPHERE SCENES FOR THE THREE POLARIMETRIC BANDS. THEY WERE COMPUTED FROM THE RTM USING THE FOLLOWING VALUES FOR THE GEOPHYSICAL PARAMETERS: SST = 25 °C, SSS = 35.0 ppt, SSWS = 7.5 m/s, COLUMNAR WATER VAPOR = 30.0 mm, AND COLUMNAR LIQUID CLOUD WATER = 0.05 mm

Band	$\partial\left(F_V - \frac{1}{2}F_H\right)\Big/\partial\theta \quad [K/\text{deg}]$	$Q \quad [K]$
10.7	2.759	69.2
18.7	2.756	72.2
37.0	2.287	59.3

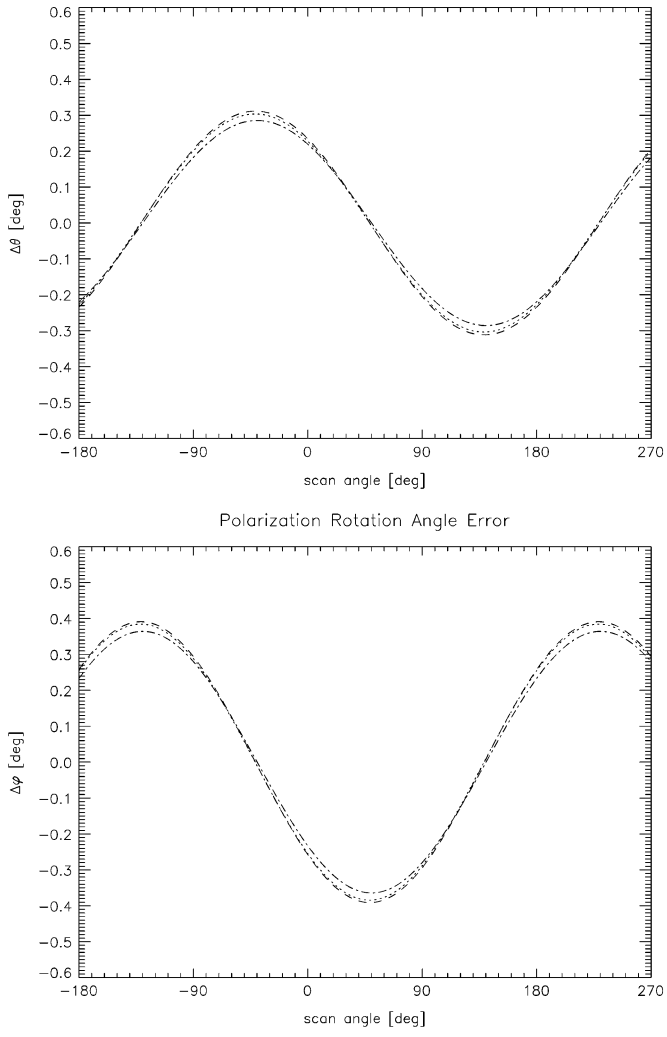

Fig. 3. Error in the EIA $\Delta\theta$ and the polarization rotation angle $\Delta\varphi$ for the orbits from Fig. 2 as function of the antenna boresight looking azimuth (scan angle) at (dotted line) 10.7, (dashed line) 18.7, and (dashed–dotted line) 37.0 GHz.

It is obvious that all the along-scan biases have basically vanished. It is very satisfying to see that the along-scan errors in all 22 WindSat channels were corrected by making a small change to the S/C roll and pitch.

The effect of this S/C roll and pitch correction to geographic contours, such as coastlines, can be easily seen from the equation for $\Delta\theta(\omega) = \theta_{\text{true}} - \theta_{\text{rep}}$ in (10). The EIA difference corresponds to a tilt of the S/C $\hat{Z}$ axis by about 0.24°. $\Delta\theta(\omega)$ reaches its largest positive value of $\Delta\theta_0 = 0.326°$ when the scan angle is $\omega = \omega_0 + 90° = -40.5°$. In other words, at a scan angle of $-40.5°$ our correction tilts the look direction up and away from the Earth by 0.326°. From our sign convention for ω (positive if looking left of forward, negative if looking right of forward), it follows, that for an ascending orbit the correction shifts coastlines to the north and east. This coincides with the findings of the coastline analysis reported in this issue [11].

IV. FARADAY ROTATION

A. General Form

The polarization vector of an electromagnetic wave of frequency ν in the microwave range that propagates from the Earth to the S/C through the geomagnetic field and the Earth's ionosphere undergoes a rotation (Faraday rotation) by the angle φ_F [12]

$$\varphi_F = \frac{135}{\nu^2} \int n_e \vec{B}_{\text{geo}} \cdot d\vec{s}. \tag{11}$$

n_e is the free ionospheric electron density, $\vec{B}_{\text{geo}}$ is the geomagnetic field vector, $\hat{k}$ is the unit vector in the propagation direction, and $d\vec{s}$ is the vector line element in the direction of propagation. The units in (11) are $[\nu] =$ Hertz, $[B_{\text{geo}}] =$ Gauss, $[n_e] = \text{m}^{-3}$, and $[ds] =$ meters. When looking into the propagation direction $\hat{k}$ of the electromagnetic wave, the electric field polarization vector rotates clockwise if $\varphi_F > 0$, i.e., if the geomagnetic field is pointing along the direction of propagation. The rotation for the rotation of the electric field is therefore

$$\begin{pmatrix} E_V \\ E_H \end{pmatrix}_F = \begin{pmatrix} \cos(\varphi_F) & -\sin(\varphi_F) \\ +\sin(\varphi_F) & \cos(\varphi_F) \end{pmatrix} \cdot \begin{pmatrix} E_V \\ E_H \end{pmatrix} \tag{12}$$

and the rotation of the Stokes parameters is

$$\begin{pmatrix} Q_F \\ U_F \end{pmatrix} = \begin{pmatrix} \cos(2\varphi_F) & -\sin(2\varphi_F) \\ +\sin(2\varphi_F) & \cos(2\varphi_F) \end{pmatrix} \begin{pmatrix} Q \\ U \end{pmatrix}. \tag{13}$$

According to (11), the magnitude of the Faraday rotation angle grows with $1/\nu^2$. For WindSat-like Earth incidence angles and all typical ocean scenes $|Q| \gg |U|$. Therefore, according to (13), for typical values of $|\varphi_F|$ the relative impact of Faraday rotation on the third Stokes parameter U is much larger than on the second Stokes parameter Q (vertical and horizontal polarizations). For the WindSat instrument, Faraday rotation plays a significant role only for the third Stokes parameter at 10.7 GHz. The situation is different and L-band frequencies (around 1.4 GHz) that are used for future ocean surface salinity missions: Soil Moisture and Ocean Salinity and AQUARIUS. At these low frequencies, the size of the Faraday rotation is more than 50 times larger than at 10.7 GHz. If not corrected, this would lead to a large relative error in the V- and H-pol brightness temperatures and therefore to inaccurate values for the ocean salinity. Several authors have modeled the impact of Faraday rotation at L-band [13]–[15]. The purpose of our study is to demonstrate how Faraday rotation

can be seen in the measured WindSat third Stokes parameter at 10.7 GHz, how it affects the wind vector retrieval, and how it can be corrected using the IRI model.

B. Faraday Rotation at 10.7 GHz for WindSat Orbits

In order to compute the Faraday rotation φ_F for WindSat orbits we assume a spherical earth (radius $R_E = 6371.2$ km) and use the thin layer approximation [13], which assumes that all electrons are concentrated at the ionospheric layer at an altitude $h_I = 400$ km above mean sea level

$$n_e(h, \mathrm{LAT}, \mathrm{LON}) = \delta(h - h_I)\mathrm{TEC} \tag{14}$$

and

$$\mathrm{TEC}(\mathrm{LAT}, \mathrm{LON}) = \int_0^{h_{\mathrm{S/C}}} dh\, n_e(h, \mathrm{LAT}, \mathrm{LON}) \tag{15}$$

is the vertical total electron content (TEC) of the ionosphere between the Earth's surface and the S/C altitude $h_{\mathrm{S/C}}$. We can then substitute the full profile integral (11) by

$$\varphi_F = \mathrm{TEC} \cdot (\vec{B}_I \cdot \hat{k}) \cdot \left.\frac{\partial s(h)}{\partial h}\right|_{h=h_I}. \tag{16}$$

$\vec{B}_I$ is the geomagnetic field at the intersection point of the line of sight with the ionospheric layer, h is the altitude above sea level, and

$$s(h) = \sqrt{(R_E + h)^2 - R_E^2 \sin^2(\theta)} - R_E \cos(\theta) \tag{17}$$

is the distance between the Earth surface and the S/C. We have evaluated the full integral in (11) using IRI electron profiles and found that approximating (11) by (16) is accurate to about 5%.

Real-time values for the TEC can be obtained from Global Positioning System (GPS) data. GPS satellites measure the time delay of an electromagnetic wave traveling through the Earth's ionosphere, which is proportional to the TEC. However, using GPS data would mean that they have to be collocated with the WindSat measurements, which makes only a small part of the swath usable. For this study, we have obtained the TEC from the International Reference Ionosphere (IRI 2001) model (http://nssdc.gsfc.nasa.gov/space/model/ionos/iri.html). The accuracy of the TEC from this model compared with real-time measurements is typical on the order of 10% to 20% [16], which translates directly into a 10% to 20% error for φ_F.

Values for the geomagnetic field have been obtained from the International Geomagnetic Reference Field (http://www.ngdc.noaa.gov/IAGA/vmod/).

Fig. 4 shows the distribution of φ_F at 10.7 GHz over the ocean for two sets, each containing 30 orbits during different time periods. The observations were averaged into target cells matching the size of the 10.7-GHz footprint. The upper panels of Fig. 5 show φ_F over the ocean for one full orbit (rev # 3733) for the forward look (left panel) and aft look (right panel). The largest negative (positive) values for φ_F occur for the forward (aft) look during the ascending swaths at low northern (southern) latitudes. This is a result of the WindSat look geometry relative to the direction of the geomagnetic field and the fact that the maximum TEC occurs near $\pm 15°$ geomagnetic latitude. The diurnal maximum (minimum) of the TEC is reached during early afternoon (early morning) hours local time. Because the WindSat

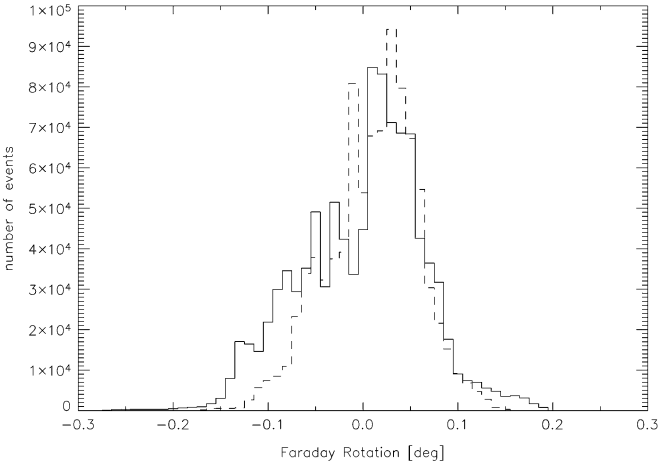

Fig. 4. Distribution of Faraday Rotation angles over the ocean for two 30-orbit periods. (Full line) Rev # 3720–rev # 3749 (September 25–27, 2003) and (dashed line) rev # 5211–rev # 5240 (January 8–10, 2004). The bin size is 0.01°. The observations were averaged into target cells matching the size of the 10.7-GHz footprint.

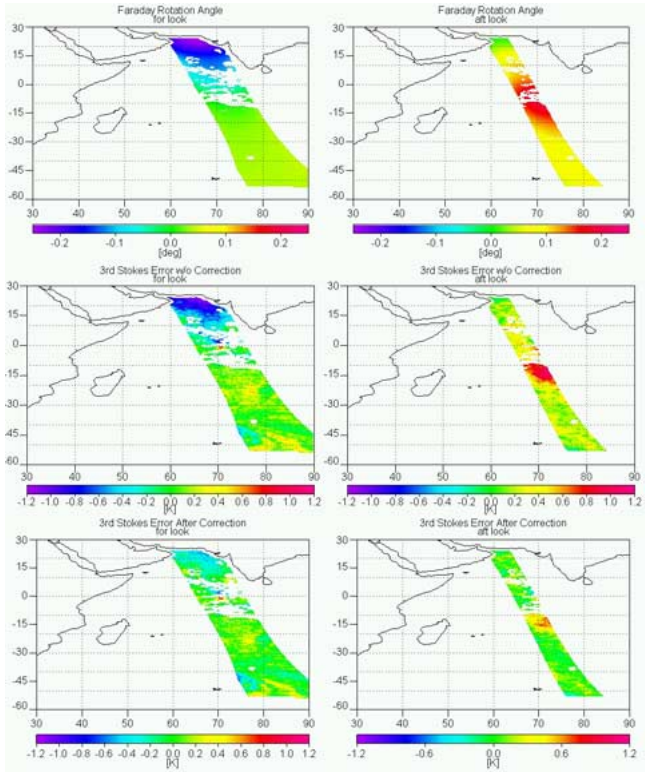

Fig. 5. Faraday rotation at 10.7 GHz and error in the 10.7-GHz third Stokes parameter (measurement minus RTM function) for orbit rev # 3733 (September 26, 2003). The left (right) panels show forward (aft) look. The upper panels show the magnitude and size of the Faraday rotation angle. The middle (lower) panels show the error in the third Stokes parameter without (with) including Faraday rotation in the polarization rotation correction.

local ascending node time is 17:59, the absolute values for φ_F tend to be larger for the ascending than for the descending part of the swath. The distributions in Fig. 4 are not symmetric around zero, because the number of Earth observations for each scan is larger during the forward look than during the aft look. During early fall larger values for φ_F occur than during winter. The reason for this is that the size of the TEC peak at $\pm 15°$ geomag-

netic latitude is larger during equinox than during solstice, because the sun radiation at low latitudes is larger during equinox than during solstice. We also want to mention that the distribution of φ_F is not completely symmetric around the Earth's rotational axis, because geomagnetic and geographic poles do not coincide. We observe larger absolute peak values for φ_F at low-mid latitudes during ascending swaths that are crossing the Indian Ocean (such as orbit rev #3733 in Fig. 5) or the western Pacific Ocean than during ascending swaths that are crossing the eastern Pacific or Atlantic Oceans.

Finally, it should be noted that the time under consideration (2003–2004) falls within a period of moderate solar activity within the 11-year solar cycle, and therefore only moderate values for the TEC and $|\varphi_F|$ are observed. When the solar activity reaches its maximum we can expect that the peak values for TEC and $|\varphi_F|$ will increase by a factor 2.

C. Impact of Faraday Rotation on the Accuracy of the Third Stokes Parameter and Wind Vector Retrievals

The general form of the relation between the Stokes vector at the ocean surface and the Stokes vector measured at the S/C when taking into account both the polarization basis rotation (7) and the Faraday rotation (13) is

$$\begin{aligned}\begin{pmatrix} Q' \\ U' \end{pmatrix} &= \begin{pmatrix} \cos(2\varphi_P) & -\sin(2\varphi_P) \\ +\sin(2\varphi_P) & \cos(2\varphi_P) \end{pmatrix} \\ &\quad \cdot \begin{pmatrix} \cos(2\varphi_F) & -\sin(2\varphi_F) \\ +\sin(2\varphi_F) & \cos(2\varphi_F) \end{pmatrix} \begin{pmatrix} Q \\ U \end{pmatrix} \\ &= \begin{pmatrix} \cos(2(\varphi_F+\varphi_P)) & -\sin(2(\varphi_F+\varphi_P)) \\ +\sin(2(\varphi_F+\varphi_P)) & \cos(2(\varphi_F+\varphi_P)) \end{pmatrix} \begin{pmatrix} Q \\ U \end{pmatrix}. \end{aligned} \tag{18}$$

The central and lower panels of Fig. 5 show the difference between the measured and computed third Stokes parameter at 10.7 GHz for the orbit rev # 3733. In the central panel, the Faraday rotation angle in (18) was ignored when computing the ocean surface third Stokes U parameter from the WindSat third Stokes U' parameter as described in Section II-B3. The result that is obtained when including φ_F is shown in the lower panel of Fig. 5. The correlation between Faraday rotation and error in the third Stokes parameter is evident.

Fig. 6 shows the impact of this error on the accuracy of the WindSat wind direction retrieval. The algorithm for retrieving wind vectors is the Ocean Suite for the Conical-Scanning Microwave Imaging Sounder (CMIS) [17] that has been adapted for the WindSat configuration. We have first neglected Faraday rotation (dashed line) and then taken it into account (full line) when doing the polarization rotation correction. The figure shows the RMS difference between the wind direction of the wind vector ambiguity that is closest to the NCEP GDAS field, which has been space-time interpolated to the WindSat observation, and the NCEP GDAS wind direction if the NCEP wind speed is larger than 5 m/s. Details of our wind vector retrieval algorithm will be reported elsewhere. We have considered 30 orbits (rev # 3720–3749) for our analysis. The result is binned as a function of the absolute value of the Faraday rotation $|\varphi_F|$ using a bin size of 0.025°. We see that for $|\varphi_F| > 0.15°$ the effect of neglecting Faraday rotation on the accuracy of the wind direction retrieval

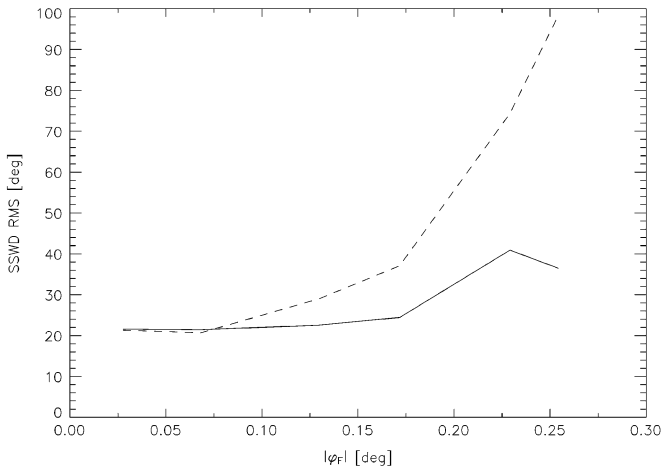

Fig. 6. RMS difference between the wind direction of the NCEP GDAS analysis and the closest ambiguity of the wind vector retrieved from WindSat for wind speeds larger than 5 m/s plotted as a function of the absolute value of the Faraday rotation angle. The computation was done for 30 orbits (rev # 3720–3749). The binsize is 0.025°. The full (dashed) line shows the result if the Faraday rotation was included (not included) in the cross-polarization correction.

is significant. In those cases, it is therefore essential to include Faraday rotation in the polarization rotation correction. During the current period of moderate solar activity within the 11-year solar cycle, those values for $|\varphi_F|$ occur relatively rarely (Fig. 4) and therefore the effect plays only a small role within global statistics containing a large number of observations. We also note that even after doing this correction, there still remains a small correlation between $|\varphi_F|$ and the wind direction error. This is a result of the fact that we have not used real-time measurements but the IRI 2001 model for the TEC when computing φ_F. Therefore, a small residual error can be expected.

V. Summary

An accurate determination of the ocean surface third Stokes parameter from WindSat measurements requires the knowledge of the rotation angle between the electric field polarization vector at the ocean surface and the S/C. This angle depends on the S/C attitude and on Faraday rotation.

An analysis of along-scan biases for $V - H/2$ as well as the third Stokes parameter revealed a misspecification of the S/C roll and pitch that were used in the WindSat TDRs [1], [2]. The error is large enough to make accurate wind vector retrievals impossible. We were able to correct the along-scan errors in all 22 WindSat channels by making a small change to the S/C roll and pitch. The same roll and pitch correction also eliminates along-scan biases in V-pol and H-pol, which arise due to a misspecification of the EIA. Based on our findings we expect the misspecification is constant and therefore these corrections will remain constant over the life of the instrument.

If not corrected, Faraday rotation angles larger than 0.15° at 10.7 GHz lead to an increase in the error of the 10.7-GHz third Stokes parameter and degrade the accuracy of wind vector retrievals. We have computed the Faraday rotation angle from the TEC of the IRI 2001 model and shown that including it in the polarization rotation correction leads to a significant improvement in those cases.

APPENDIX
SPACECRAFT ATTITUDE AND GEOLOCATION

This Appendix briefly summarizes our conventions and specifications and the main steps for geolocation and the computation of EIA and polarization rotation angle.

The axes $\{\hat{E}_1, \hat{E}_2, \hat{E}_3\}$ of the geocentric-equatorial coordinate system [18] are as follows.

1) $\hat{E}_3$ points along the Earth rotation axis from south to north.
2) $\hat{E}_1$ lies in the equatorial plane. It points into the direction of the vernal equinox for an inertial system and into the direction of the Greenwich meridian for a system rotating with the Earth.
3) $\hat{E}_2$ completes the right-hand system.

The S/C coordinate vector $\vec{R}_{\mathrm{S/C}}$ in the $\{\hat{E}_1, \hat{E}_2, \hat{E}_3\}$ system is

$$\vec{R}_{\mathrm{S/C}} = \begin{pmatrix} r_1 \\ r_2 \\ r_3 \end{pmatrix} \cdot \hat{R}_{\mathrm{S/C}} = \begin{pmatrix} \left[\frac{\rho_e}{\sqrt{1-\varepsilon^2 \sin^2(\Theta_{\mathrm{S/C}})}} + h_{\mathrm{S/C}}\right] \cos(\Theta_{\mathrm{S/C}}) \cos(\Phi_{\mathrm{S/C}}) \\ \left[\frac{\rho_e}{\sqrt{1-\varepsilon^2 \sin^2(\Theta_{\mathrm{S/C}})}} + h_{\mathrm{S/C}}\right] \cos(\Theta_{\mathrm{S/C}}) \sin(\Phi_{\mathrm{S/C}}) \\ \left[\frac{\rho_e(1-\varepsilon^2)}{\sqrt{1-\varepsilon^2 \sin^2(\Theta_{\mathrm{S/C}})}} + h_{\mathrm{S/C}}\right] \sin(\Theta_{\mathrm{S/C}}) \end{pmatrix}. \quad (19)$$

$R_{\mathrm{S/C}} = |\vec{R}_{\mathrm{S/C}}| = \sqrt{(r_1^2 + r_2^2 + r_3^2)}$ is the distance from the S/C to the Earth center, $h_{\mathrm{S/C}}$ is the S/C altitude, and $\Theta_{\mathrm{S/C}}$ is the geodetic S/C latitude. In the Earth-fixed system, $\Phi_{\mathrm{S/C}}$ is identical to the S/C longitude $\lambda_{\mathrm{S/C}}$. In the inertial system $\Phi_{\mathrm{S/C}} = \lambda_{\mathrm{S/C}} + \Omega(\Delta t)$, where $\Omega(\Delta t)$ is the Earth rotation angle during the time interval Δt between the last crossing of the Greenwich meridian of the vernal equinox direction and the time of observation. $\rho_e = 6378.137$ km is the Earth equatorial radius, $\rho_p = 6356.824$ km is the Earth polar radius, and $\varepsilon^2 = 1 - (\rho_p^2)/(\rho_e^2)$.

For the geocentric WindSat mission the directions of the spacecraft nominal axes (no roll, pitch, or yaw) $\{\hat{X}_0, \hat{Y}_0, \hat{Z}_0\}$ are as follows.

1) $\hat{Z}_0$ is pointing upward from the Earth center to the S/C.
2) $\hat{Y}_0$ is pointing into the direction of the orbital angular momentum.
3) $\hat{X}_0 = \hat{Y}_0 \times \hat{Z}_0$.

The attitude matrices for the three Euler angles roll r, pitch p, and yaw y are defined as

$$R(r) = \begin{pmatrix} 1 & 0 & 0 \\ 0 & \cos(r) & \sin(r) \\ 0 & -\sin(r) & \cos(r) \end{pmatrix} \quad \text{roll matrix}$$

$$R(p) = \begin{pmatrix} \cos(p) & 0 & \sin(p) \\ 0 & 1 & 0 \\ -\sin(p) & 0 & \cos(p) \end{pmatrix} \quad \text{pitch matrix}$$

$$R(y) = \begin{pmatrix} \cos(y) & -\sin(y) & 0 \\ \sin(y) & \cos(y) & 0 \\ 0 & 0 & 1 \end{pmatrix} \quad \text{yaw matrix.} \quad (20)$$

The total attitude matrix is the product

$$R(r,p,y) = R(r) \cdot R(p) \cdot R(y). \quad (21)$$

If we denote the components of the nominal S/C axes $\{\hat{X}_0, \hat{Y}_0, \hat{Z}_0\}$ in terms of the geocentric-equatorial system $\{\hat{E}_1, \hat{E}_2, \hat{E}_3\}$ as x_{0i}, y_{0i} and $z_{0i}, i = 1,2,3$, then the components of the real S/C axes $\{\hat{X}, \hat{Y}, \hat{Z}\}$ (after roll, pitch, and yaw are included) in terms of $\{\hat{E}_1, \hat{E}_2, \hat{E}_3\}$ are

$$\begin{pmatrix} x_i \\ y_i \\ z_i \end{pmatrix} = R(r,p,y) \cdot \begin{pmatrix} x_{0i} \\ y_{0i} \\ z_{0i} \end{pmatrix}, \qquad i = 1,2,3. \quad (22)$$

The boresight unit vector $\hat{b} = b_1\hat{E}_1 + b_2\hat{E}_2 + b_3\hat{E}_3$ pointing from the S/C to the Earth cell has the $\{\hat{X}, \hat{Y}, \hat{Z}\}$ decomposition

$$\hat{b} = \sin(\theta_n) \cdot \cos(\omega) \cdot \hat{X} + \sin(\theta_n) \cdot \sin(\omega) \cdot \hat{Y} - \cos(\theta_n) \cdot \hat{Z} \quad (23)$$

where θ_n is the boresight nadir angle of the feedhorn and ω is the boresight looking azimuth (scan angle). The coordinate vector $\vec{R}_E$ of the boresight–Earth intersection point in the $\{\hat{E}_1, \hat{E}_2, \hat{E}_3\}$ system is

$$\vec{R}_E = \begin{pmatrix} \left[\frac{\rho_e}{\sqrt{1-\varepsilon^2 \sin^2(\Theta_E)}}\right] \cos(\Theta_E) \cos(\Phi_E) \\ \left[\frac{\rho_e}{\sqrt{1-\varepsilon^2 \sin^2(\Theta_E)}}\right] \cos(\Theta_E) \sin(\Phi_E) \\ \left[\frac{\rho_e(1-\varepsilon^2)}{\sqrt{1-\varepsilon^2 \sin^2(\Theta_E)}}\right] \sin(\Theta_E) \end{pmatrix}. \quad (24)$$

Θ_E and λ_E are geodetic latitude and longitude of the Earth observation cell, respectively, and $\Phi_E = \lambda_E + \Omega(\Delta t)$. The components of $\vec{R}_E$ can be computed from

$$\vec{R}_E = \vec{R}_{\mathrm{S/C}} + \eta \cdot \hat{b} \quad (25)$$

where

$$\eta = R_{\mathrm{S/C}} \cdot [B - \sqrt{B^2 - C}] \quad (26)$$

is the range distance from the S/C to the Earth cell and

$$B = -\frac{r_1 b_1 + r_2 b_2 + \left(\frac{\rho_e}{\rho_p}\right)^2 r_3 b_3}{1 + \left[\left(\frac{\rho_e}{\rho_p}\right)^2 - 1\right] b_3^2}$$

$$C = \frac{1 - \left(\frac{\rho_e}{\rho_p}\right)^2 + \left[\left(\frac{\rho_e}{\rho_p}\right)^2 - 1\right] b_3^2}{1 + \left[\left(\frac{\rho_e}{\rho_p}\right)^2 - 1\right] b_3^2}. \quad (27)$$

At the boresight–Earth intersection point, we can form a local coordinate system $\{\hat{S}, \hat{E}, \hat{U}\}$ consisting of the following:

1) surface normal $\hat{U}$ pointing upward from the Earth;
2) vector $\hat{S}$ pointing north to south along the local meridian;
3) vector $\hat{E}$ pointing locally east parallel to the equator.

The components of $\{\hat{S}, \hat{E}, \hat{U}\}$ in the $\{\hat{E}_1, \hat{E}_2, \hat{E}_3\}$ system are

$$\begin{aligned} \hat{U} &= \cos(\Theta_E)\cos(\Phi_E)\hat{E}_1 + \cos(\Theta_E)\sin(\Phi_E)\hat{E}_2 \\ &\quad + \sin(\Theta_E)\hat{E}_3 \\ \hat{E} &= -\sin(\Phi_E)\hat{E}_1 + \cos(\Phi_E)\hat{E}_2 \\ \hat{S} &= \hat{E} \times \hat{U}. \end{aligned} \quad (28)$$

The components of $\hat{b}$ in the $\{\hat{S}, \hat{E}, \hat{U}\}$ system are

$$\hat{b} = -\sin(\theta)\cdot\cos(\alpha)\cdot\hat{S} + \sin(\theta)\cdot\sin(\alpha)\cdot\hat{E} - \cos(\theta)\cdot\hat{U} \quad (29)$$

where θ is the Earth incidence angle (EIA) and α is the looking azimuth relative to north.

The polarization basis vectors at the Earth surface are

$$\hat{H} = \frac{\hat{k}\times\hat{U}}{|\hat{k}\times\hat{U}|} \qquad \hat{V} = \hat{H}\times\hat{k}. \quad (30)$$

The polarization basis vectors in the S/C system are

$$\hat{H}' = \frac{\hat{k}\times\hat{Z}}{|\hat{k}\times\hat{Z}|} \qquad \hat{V}' = \hat{H}'\times\hat{k}. \quad (31)$$

$\hat{k} = -\hat{b}$ is the propagation direction of the electromagnetic wave from the Earth observation cell to the S/C. This defines the polarization rotation angle φ_P between the Earth and S/C polarization bases

$$\begin{pmatrix}\hat{V}'\\ \hat{H}'\end{pmatrix} = \begin{pmatrix}(\hat{V}'\cdot\hat{V}) & (\hat{V}'\cdot\hat{H})\\ (\hat{H}'\cdot\hat{V}) & (\hat{H}'\cdot\hat{H})\end{pmatrix}\cdot\begin{pmatrix}\hat{V}\\ \hat{H}\end{pmatrix} = \begin{pmatrix}\cos(\varphi_P) & -\sin(\varphi_P)\\ +\sin(\varphi_P) & \cos(\varphi_P)\end{pmatrix}\cdot\begin{pmatrix}\hat{V}\\ \hat{H}\end{pmatrix}. \quad (32)$$

REFERENCES

[1] P. Gaiser *et al.*, "The Windsat spaceborne polarimetric microwave radiometer: Sensor description and early orbit performance," *IEEE Trans. Geosci. Remote Sens.*, vol. 42, no. 11, pp. 2347–2361, Nov. 2004.

[2] P. Gaiser, "WindSat TDR version 146AFBBDA. Data and format description," Nav. Res. Lab., Washington, DC, Dec. 2003.

[3] P. Gaiser, "WindSat antenna pattern correction description. Report and Data," Nav. Res. Lab., Washington, DC, Mar. 2003.

[4] F. Wentz and T. Meissner, "AMSR ocean algorithm. Algorithm Theoretical Basis Document (ATBD)," Remote Sens. Syst., Santa Rosa, CA, ser. 2, Dec. 1999.

[5] T. Meissner and F. Wentz, "An updated analysis of the wind direction signal in passive microwave brightness temperatures," *IEEE Trans. Geosci. Remote Sens.*, vol. 40, no. 6, pp. 1230–1240, Jun. 2002.

[6] S. Yueh and W. Wilson, Validation of wind radiometer technique using aircraft radiometer and radar measurements for high ocean Winds, Jet Propulsion Lab., Pasadena, CA, 1999.

[7] R. W. Reynolds and T. M. Smith, "Improved global sea surface temperature analyses using optimum interpolation," *J. Clim.*, vol. 7, pp. 929–948, 1994.

[8] NODC, *World Ocean Atlas 1998 (WOA98)*. Silver Spring, MD: Ocean Climate Lab., Nat. Oceanogr. Data Center, 1998. CD-ROM.

[9] F. Wentz and R. Spencer, "SSM/I rain retrievals within a unified all-weather ocean algorithm," *J. Atmos. Sci.*, vol. 55, no. 9, pp. 1613–1627, 1998.

[10] I. Corbella *et al.*, "Compensation of elevation angle variations in polarimetric brightness temperature measurements from airborne microwave radiometers," *IEEE Trans. Geosci. Remote Sens.*, vol. 39, no. 1, pp. 193–195, Jan. 2001.

[11] W. Purdy *et al.*, "Geolocation and pointing accuracy analysis for the Windsat sensor," *IEEE Trans. Geosci. Remote Sens.*, vol. 44, no. 3, pp. 496–505, Mar. 2006.

[12] G. Rybicki and A. Lightman, *Radiative Processes in Astrophysics*. New York: Wiley, 1979.

[13] D. Le Vine and S. Abraham, "Faraday Rotation and passive microwave remote sensing of soil moisture from space," in *Microwave Radiometry Remote Sensing Earth's Surface Atmosphere*, P. P. A. S. Paloscia, Ed. Leiden, The Netherlands: VSP, 2000, pp. 89–96.

[14] D. Le Vine and S. Abraham, "The effect of the ionpsphere on remote sensing of sea surface salinity From Space: Absorption and emission at L Band," *IEEE Trans. Geosci. Remote Sens.*, vol. 40, no. 4, pp. 771–782, Apr. 2002.

[15] S. Abraham and D. L. Vine, "Use of IRI to model the effect of ionospheric emission on earth remote sensing at L-band," *Adv. Space Res.*, vol. 34, pp. 2059–2066, 2004.

[16] A. Komjathy, R. B. Langley, and D. Bilitza, "Ingesting GPS-derived TEC data into the international reference ionosphere for single frequency radar altimeter ionospheric delay corrections," *Adv. Space Res.*, vol. 22, no. 6, pp. 793–801, 1998.

[17] T. Meissner and F. Wentz, "The ocean algorithm suite for the Conical-Scanning Microwave Imager (CMIS)," *Proc. IGARSS*, 2002.

[18] O. Montenbruck and E. Gill, *Satellite Orbits: Models, Methods, and Applications*. Berlin, Germany: Springer-Verlag, 2000.

Thomas Meissner received the B.S. degree in physics from the University of Erlangen-Nürnberg, Nürnberg, Germany, the M.S. degree (Diploma) in physics from the University of Bonn, Bonn, Germany, and the Ph.D. degree in theoretical physics from the University of Bochum, Bochum, Germany, in 1983, 1987, and 1991, respectively. He wrote his doctoral dissertation on effective quark models of the nucleon.

Between 1992 and 1998, he conducted postdoctoral research at the University of Washington, Seattle, the University of South Carolina, Columbia, and Carnegie Mellon University, Pittsburgh, PA, in theoretical nuclear and particle physics, focusing on the theory of strong interaction. Since July 1998, he has been with Remote Sensing Systems, Santa Rosa, CA. Since then, he has been working on the development and refinement of radiative transfer models, calibration, validation, and ocean retrieval algorithms for various microwave instruments (SSM/I, TMI, AMSR-E, WindSat, CMIS).

Frank J. Wentz received the B.S. and M.S. degree in physics from Massachusetts Institute of Technology, Cambridge, MA, in 1969 and 1971, respectively.

In 1974, he established Remote Sensing Systems (RSS), Santa Rosa, CA, a research company specializing in satellite microwave remote sensing of the Earth. His research focuses on radiative transfer models that relate satellite observations to geophysical parameters, with the objective of providing reliable geophysical datasets to the Earth Science community. As a member of the National Aeronautics and Space Administration's (NASA) SeaSat Experiment Team (1978–1982), he pioneered the development of physically based retrieval methods for microwave scatterometers and radiometers. Starting in 1987, he took the lead on providing the world-wide research community with high-quality ocean products derived from satellite microwave imagers (SSM/I). As the Director of RSS, he overseas the production and validation of reliable scatterometer and radiometer products. These data are dispersed via the company's web and ftp sites. He is currently a member of NASA Earth Observation System Investigators Working Group, NASA Advanced Microwave Scanning Radiometer Team, NASA Ocean Vector Wind Science Team, NASA Tropical Rainfall Mission Team, and NASA Pathfinder Activity. He is currently working on scatterometer/radiometer combinations, satellite-derived decadal time series of atmospheric moisture and temperature, the measurement of sea-surface temperature through clouds, and advanced microwave sensor designs for climatological studies

Mr. Wentz has served on many NASA review panels, the National Research Council's Earth Studies Board, the National Research Council's Panel on Reconciling Temperature Observations, and is a member of the American Geophysical Union.